

The NEXT experiment for $\beta\beta0\nu$ searches at LSC

A status report: April 2016

THE NEXT COLLABORATION

April 19, 2016

Contents

1	Introduction	2
2	The NEXT Infrastructures	3
3	The NEW detector	18
3.1	Energy Plane	18
3.2	Tracking Plane	18
3.3	Field Cage	29
4	Conclusions	36

1 Introduction

The goal of the *Neutrino Experiment with a Xenon TPC* (**NEXT**)¹ project is the construction, commissioning and operation of the NEXT-100 detector, a high-pressure, xenon (HPXe) Time Projection Chamber using electroluminescent (EL) readout. NEXT-100 will search for neutrinoless double beta decay ($\beta\beta0\nu$) events in ^{136}Xe , deploying 100 kg of xenon enriched at 90% in the isotope ^{136}Xe . The host of the experiment is the Canfranc Underground Laboratory (LSC).

The project is being developed in three stages. A first R&D stage extended from 2010 to 2015. Three 1-kg xenon prototypes, NEXT-DBDM (LBNL), NEXT-DEMO (IFIC) and NEXT-MM (Zaragoza), have shown the excellent performance (energy resolution, electron reconstruction) of the chosen EL technology, as well as explored alternative options such as operation with gain (using Micromegas readout) in xenon-TMA mixtures. Some of the most important results include:

1. The design and characterisation of the SiPM tracking system [1].
2. PMT calibration in situ procedures [2].
3. The procedures and results of the radiopurity campaign for NEXT-100 [3–5].
4. Description of the trigger system for NEXT-DEMO (and its extrapolation to NEXT-100) [6].
5. Description of the front-end electronics for energy measurements [7].
6. Performance of EL prototypes [8–11].
7. Initial results on operation with Xe-TMA mixtures [12, 13].
8. Measurements with alpha particles and nuclear recoils [14, 15].
9. Topological signature [16].
10. Physics potential of the detector [17–20].

The second stage of the project is the construction, commissioning and operation of NEW (NEXT-WHITE)², a first-stage, radiopure, 10-kg demonstrator intended to exercise the NEXT-100 detector technical solutions and infrastructures (including the gas system and the Slow Controls), as well as to provide essential data for the NEXT background model. NEW and the infrastructures have been built during 2015 and 2016 is currently being commissioned at the LSC. The foreseen operation period is two years (2017 and 2018).

¹<http://next.ific.uv.es/next>

²The name honours the memory of Professor James White, recently deceased and one of the key scientists of the NEXT Collaboration.

The third stage is the construction, commissioning and operation of NEXT-100. The collaboration intends to present an updated Technical Design Report (TDR) to the LSC Scientific Committee in November-2017, seeking for approval to start construction of NEXT-100. The assembly of the NEXT-100 detector is foreseen to occur during 2018, and commissioning is expected in 2019. If the background model expectations are confirmed, NEXT-100 could improve the sensitivity of both EXO-100 and KamLAND-Zen in 2–3 years of data taking [20].

In this report we present an overview of the NEW project as of May 2016, stressing the achievements during 2015. The report is organised as follows. Section 2 describe the infrastructures needed at the LSC for the operation of the two stages of the NEXT experiment. Most of those infrastructures have been built or completed during 2015. Section 3 presents the status of the NEW apparatus, which has also been assembled during 2015. Conclusions are presented in section 4.

2 The NEXT Infrastructures

Figure 1 shows the layout of the experimental area. All the system is deployed on a working platform, made of Tramex of $11 \times 11\text{m}^2$ shown in figure 3. The NEW detector is hosted inside a lead castle (figure 4) and sitting in a seismic platform (figure 5). The seismic pedestal is frame with rectangular beams and 8 isolator seismic blocks. The pedestal is designed to swing without breaking in the event of earthquakes one order of magnitude larger than the maximum earthquake recorded in Canfranc.

The lead castle is made of lead blocks placed into a steel frame. The blocks are organised in a staggered structure to maximise the amount of lead seen by the external radiation. Additional steel sheets (made of radiopure steel-Ti alloy) provide the needed rigidity to avoid creep. The total weight of the lead is about 58 tons.

The platform and seismic pedestal were built in 2014. The lead castle has been completed in 2015.

The gas system

Xenon circulates through the detector via a gas recirculation and purification system (figure 6).

The goal of the gas system (GS) is to purify the xenon gas used by the NEXT detectors, reducing the traces of gases such as O, CO₂, CO, H₂, N₂, CH₄ and water vapour to less than one part per billion (ppb). Both NEW and NEXT-100 will operate with natural xenon (NXe) and enriched xenon (EXe). The gas will be maintained at room temperature and 10–15 bar pressure inside the detector(s). The gas system has been designed to avoid significant losses of xenon under all foreseeable circumstances.

Figure 6 shows a schematics of the gas system. Its main components (figure 7) are:

- Emergency recovery system.
- Pressure vessel (NEW or NEXT-100).

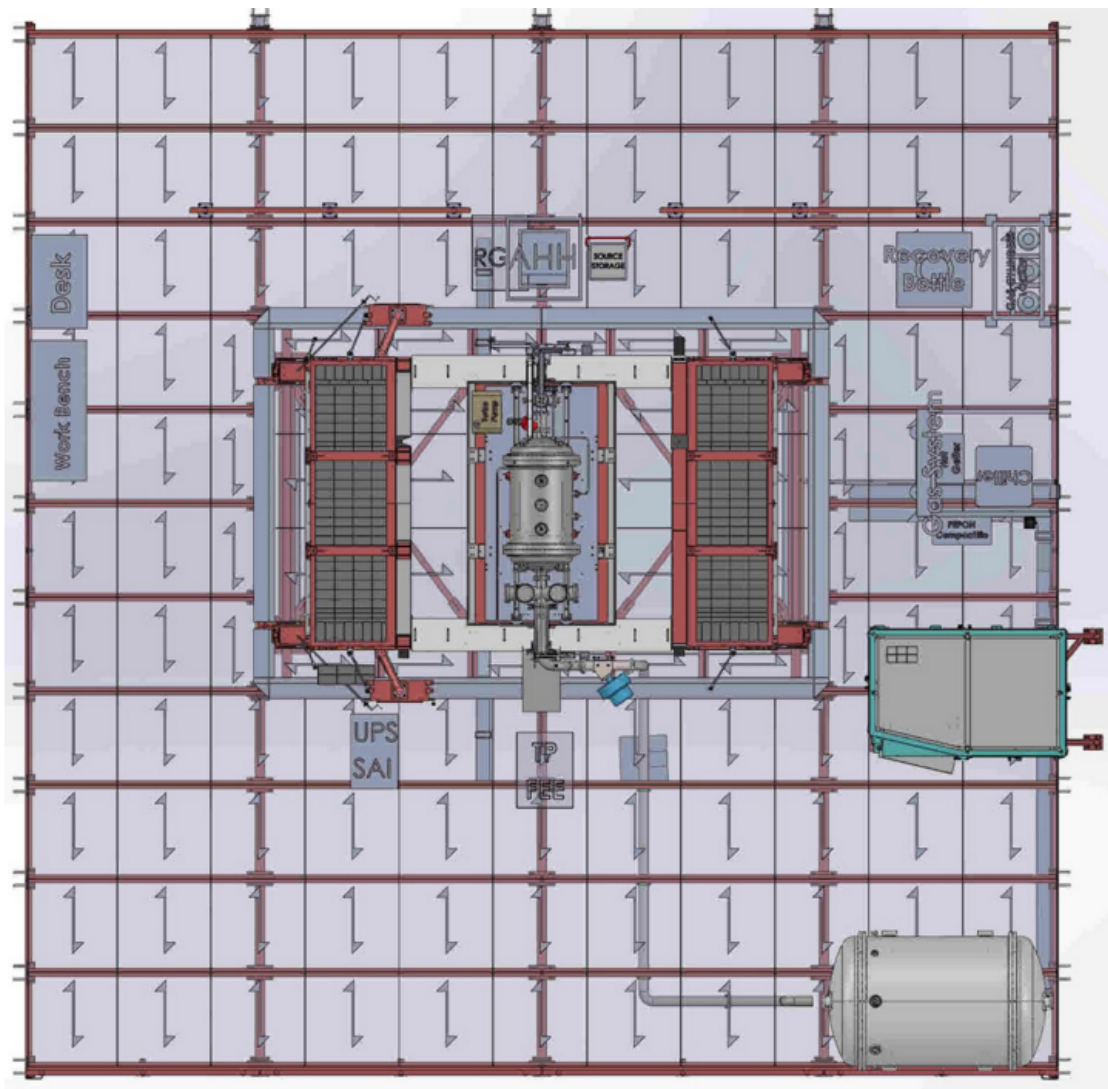


Figure 1: *Layout of the NEXT working platform.*



Figure 2: *The NEXT working platform, empty*



Figure 3: *The NEXT working platform, with infrastructures installed*

- Compressor.
- Purification loop.
- Cryo-recovery.
- Argon/xenon bottles.
- Pipes.
- Control System.

The pipes are all plumed together using ?? and 1? stainless tube and flexible hoses where mechanical insulation is required. The total amount of gas in the supply bottle and also in the system will be such that in the event of the entire bottle emptying into the system and being vented into the emergency recovery tank the final pressure will not exceed 3 bar.

Emergency recovery tank and ancillary systems

The emergency recovery section of the gas system (figure 8) is designed to recover gas into a recovery tank in the event of over pressure in the gas system. During the operation of NEW, the existing pressure vessel of the NEXT-100 experiment (a tank with a volume of



Figure 4: *The lead castle in open position*

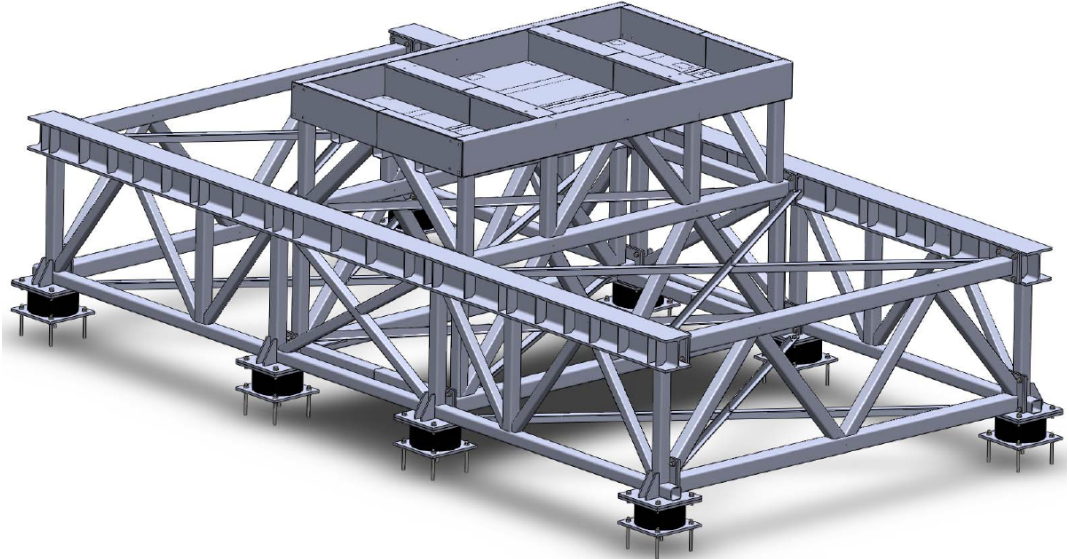


Figure 5: A 3D view of the Seismic Pedestal (SP).

2.560 m^3 made of 316Ti alloy and with CE certification for operation at 15 bar) is reused as recovery tank (figure 9). In order to guarantee that gas is dumped into the recovery tank in the event of an over-pressure, the tank is kept during normal operations at 10^{-5} mbar. This is done by pumping the tank with the vacuum pump PUMP1 (figure 10) through valves GV1 (this is a pneumatic-activated guillotine valve, certified to separate pressure from vacuum zones) and the manual valve GV2 which acts as a backup. The system is backed by a third pneumatic valve, BiVal. A pressure gauge (PG1) and a vacuum gauge (VG1) measure the pressure and vacuum in the recovery tank. A bursting disk installed in the recovery tank (BD1) will burst at 5 bar, avoiding any over-pressure in the system (notice that a pressure of 5 bar in the emergency recovery tank is equivalent to a pressure of 50 bar in the NEW pressure tank which is the maximum pressure that the vessel can tolerate).

In normal operations, the vacuum pump (PUMP1) is pumping the recovery tank and GV1 is opened. The valve is automatically controlled by the Slow Control System and to be open needs a pneumatic pressure of 4.5-5 bar and a voltage of 24 VDC. This implies that the valve closes in failure (electrical or pneumatic shutdown at the experiment or the LSC). Also, if an emergency condition (need to recover the gas) arises, PUMP1 is turned off and GV1 closes. Emergency conditions are normally triggered by excess pressure in the NEW pressure vessel. In this case, the Carten Valve opens up and as GV2 is always open, the gas will evacuate to the tank through the safety evacuation line. A second pneumatic valve, SV6 is controlled by the Slow Control System and will open up in the event of excess pressure. If both the Carten valve and SV6 fail, disk BD2 will burst at 13 bar.

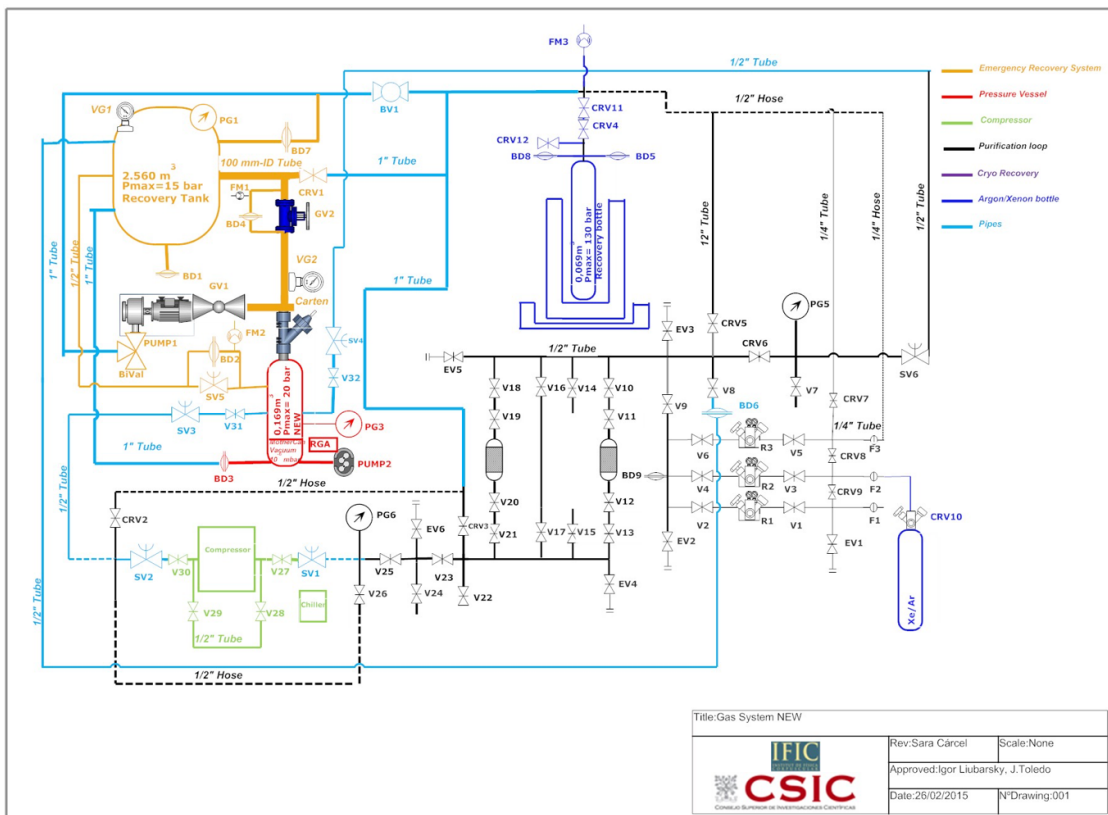


Figure 6: A functional schema of the NEXT Gas System

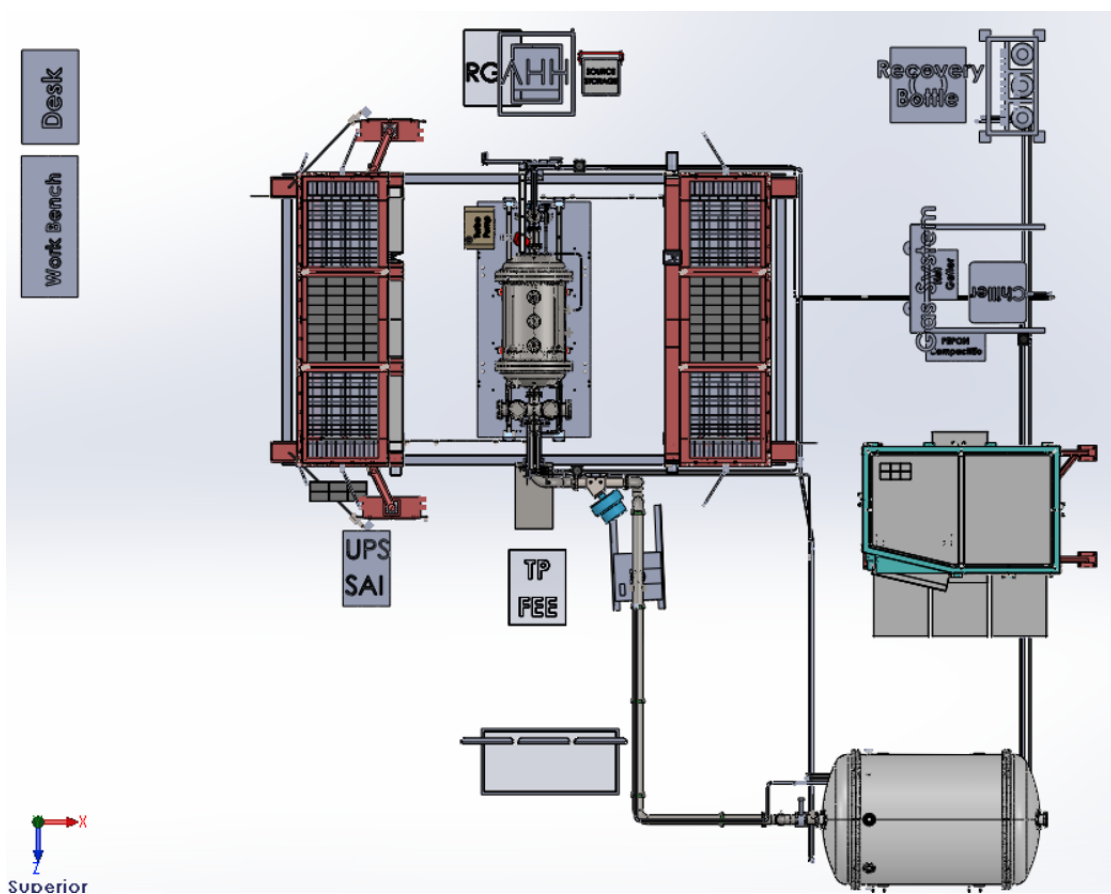


Figure 7: Drawing showing the main components of the NEXT gas system.

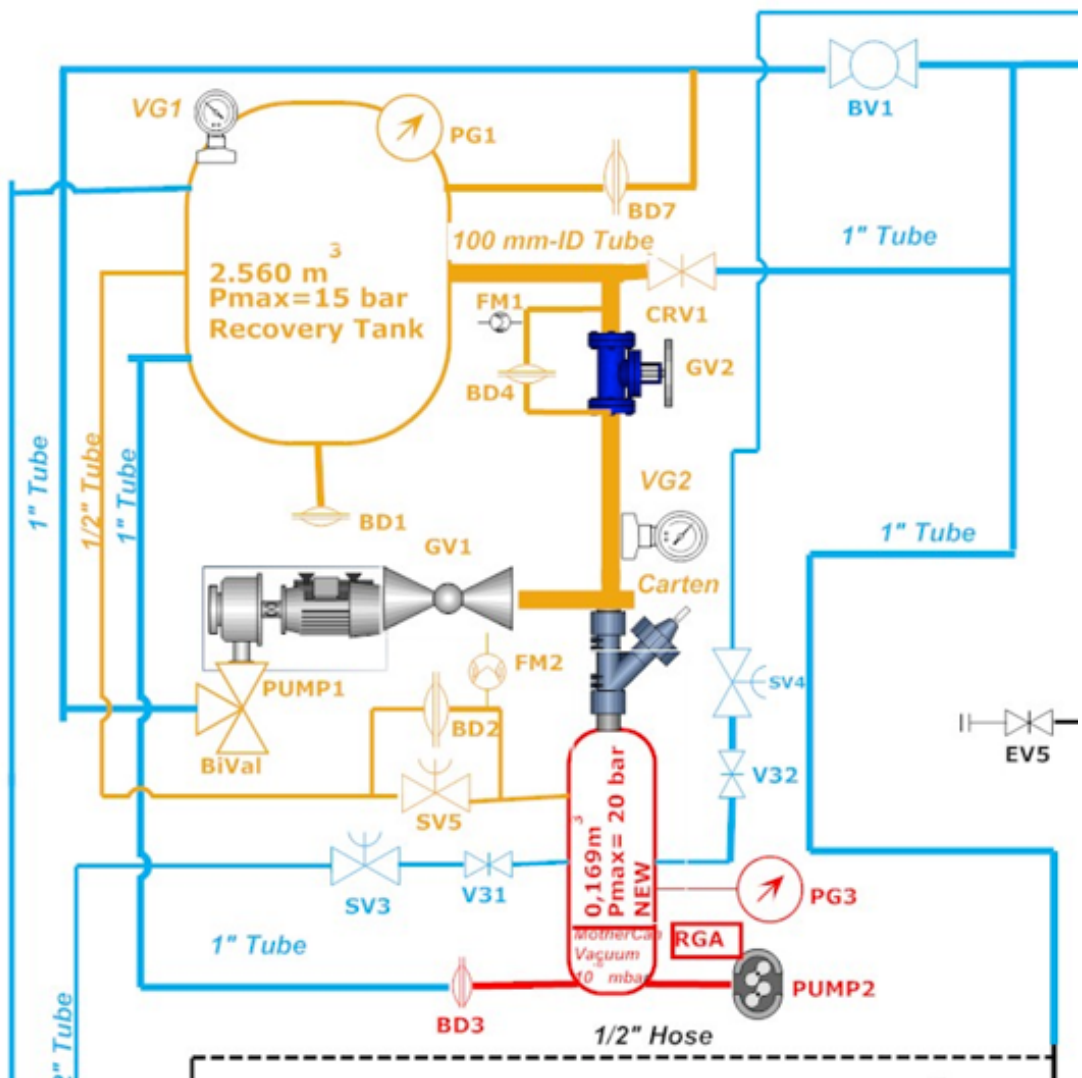


Figure 8: Emergency Recovery part of the Gas System



Figure 9: *The NEXT-100 pressure vessel operating as Emergency Recovery Tank.*



Figure 10: *A picture of the vacuum pump (PUMP1) used to keep the recovery tank at a nominal pressure of 10^{-5} mbar. The pump is sitting under the working platform.*

Recirculation compressor

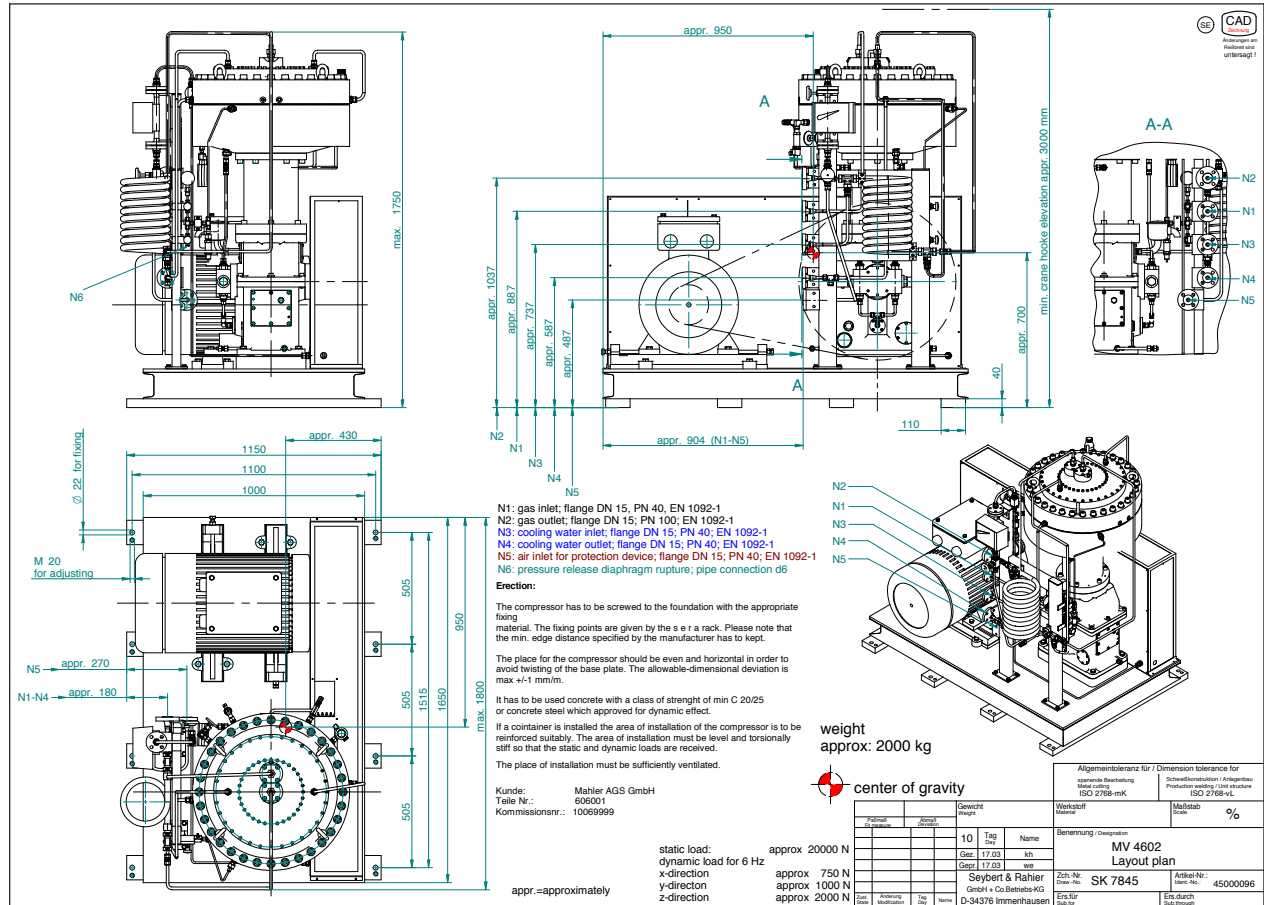


Figure 11: Schematics of the SERA recirculation compressor, chosen by NEXT.

The most vulnerable component of the gas system is the compressor, which acts as a re-circulation pump. The enriched xenon is very expensive and therefore the pump to move the gas through the re-circulation loop must have sufficient redundancy to minimise the probability of failure and leakage. Furthermore, to preserve the purity of the gas all metal to metal seals must be used.

Figure 11 shows the schematics of the compressor chosen for NEXT, manufactured by the SERA company, in Germany. The pump is made with metal-to-metal seals on all the wetted surfaces. The gas is moved through the system by a triple stainless steel diaphragm. Between each of the diaphragms there is a sniffer port to monitor for gas leakages. In the event of a leakage automatic emergency shutdown can be initiated. Figure 12 shows a picture of the compressor, already installed at the LSC.



Figure 12: A picture of the compressor.



Figure 13: The PS4-MT50 SAES hot getter chosen to purify the gas.

Hot getter

SAES PS4-MT50 hot getter (figure 13) has been chosen as the main purification filter for the xenon gas. The getter is capable of removing electron negative impurities to less than 1 ppb and deploys a nominal flow rate of 150 slpm, offering sufficient spare capacity. The gas system will contain two such getters in parallel with a bypass. The advantage of hot getter technology is their capability to remove nitrogen and methane (in addition to oxygen, water and carbon dioxide). Furthermore, hot getters are known to emit less radon than cold getters.

Recirculation loop and cryo-recovery

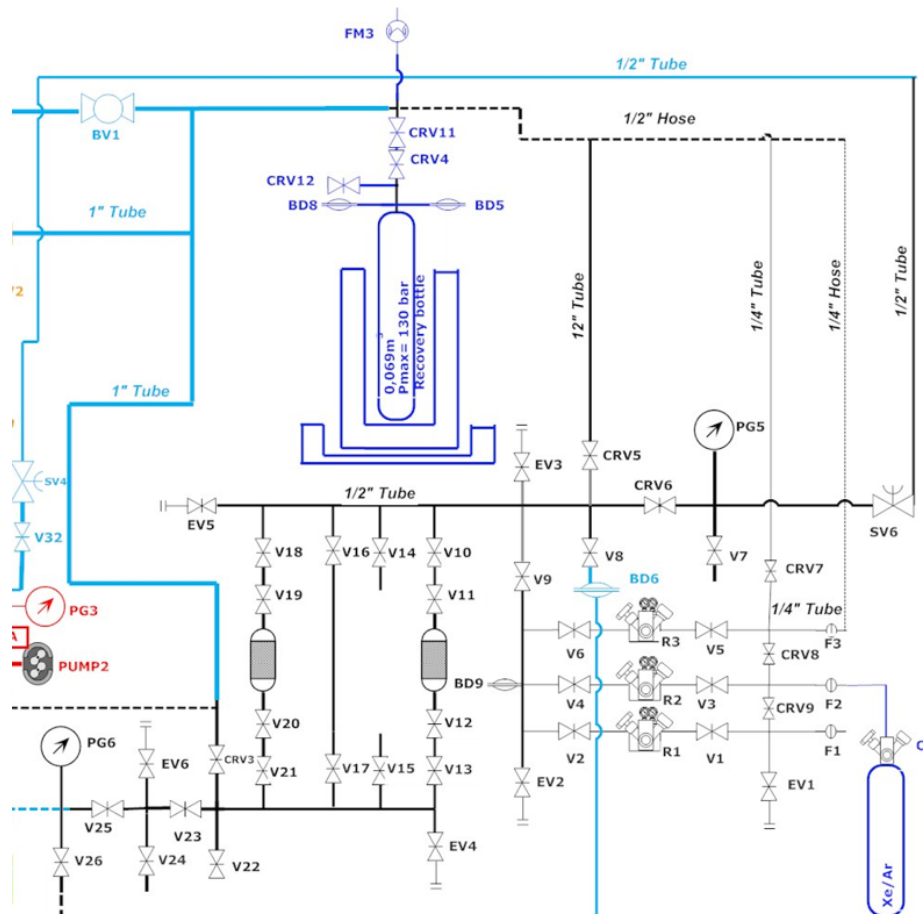


Figure 14: An scheme of the recirculation loop and cryo-recovery part of the gas system.

Figure ?? shows the recirculation loop. The gas enter the system from the pressure bottles, through a regulator and circulates through cold and/or hot getters. To recover the gas in normal conditions we use a permanently chamber cooled by liquid Nitrogen (cryo-recovery or CR), also shown in figure ??.

Summary

The needed infrastructures for the NEXT experiment have been completed during 2015 and the first quarter of 2016. The gas system is now in the final commissioning phase, and ready to pass the tests needed for underground operation certification.

3 The NEW detector

The NEW detector, shown in figure 15 is the first stage of the NEXT experiment. The NEW pressure vessel (NPV) and field cage (NFC) dimensions are roughly 1:2 with respect to those of NEXT-100. It deploys 20 % of the NEXT-100 sensors and the xenon mass is about 10 kg at 15 bar.

The primary goal of NEW is to provide an extra step in the construction of the NEXT-100 detector that allows the validation of the technological solutions proposed in the TDR. In addition, NEW will permit a measurement of the energy resolution at high energy, and the precise characterisation of the 2-electron topological signature, by measuring the $\beta\beta2\nu$ mode. Last but not least, NEW will permit a realistic assessment of the NEXT background model before the construction of the NEXT-100 detector.

Figure 16 shows the assembly of NEW at the LSC clean room during 2015. The detector has three main parts called *Energy Plane* (EP), *Tracking Plane* (TP) and *Field Cage* (FC). The EP and TP are already installed in the NEW pressure vessel. The FC will be installed during the first week of May 2016.

3.1 Energy Plane

The energy plane is shown in figure 17 and pictures of the installation in 2015 are shown in figure 18. It consists of a 11 cm thick copper support plate (called mother-can) with 12 copper window covered with brazed sapphire windows fixed to the front of the plate. The set-up as a whole seals the pressure vessel from the PMT-region, which is held at vacuum levels of $< 10^{-4}$ mbar. Additional copper shielding fixed to the vacuum side of the apertures, offer further shielding against gammas traversing the PMTs and entering in the detector volume. The 12 Hamamatsu R11410 PMTs are optically coupled to the sapphire window using NyoGel OCK-451. The sensors are held in place by a plastic brace and spring.

The PMTs receive high voltage and have their signal extracted via a shielded twisted pair cable connected to a feedthrough in the energy-plane head. The distribution of signal and supply at each individual PMT is controlled via a Kapton circuit board (base), covered with a copper cap filled with epoxy and connected to the support plate. The cap acts as a heat sink.

3.2 Tracking Plane

The NEW tracking plane, shown in figure 19 permits the reconstruction of the trajectories of charged particles, in particular electrons, in the NEW/NEXT detectors. It consists

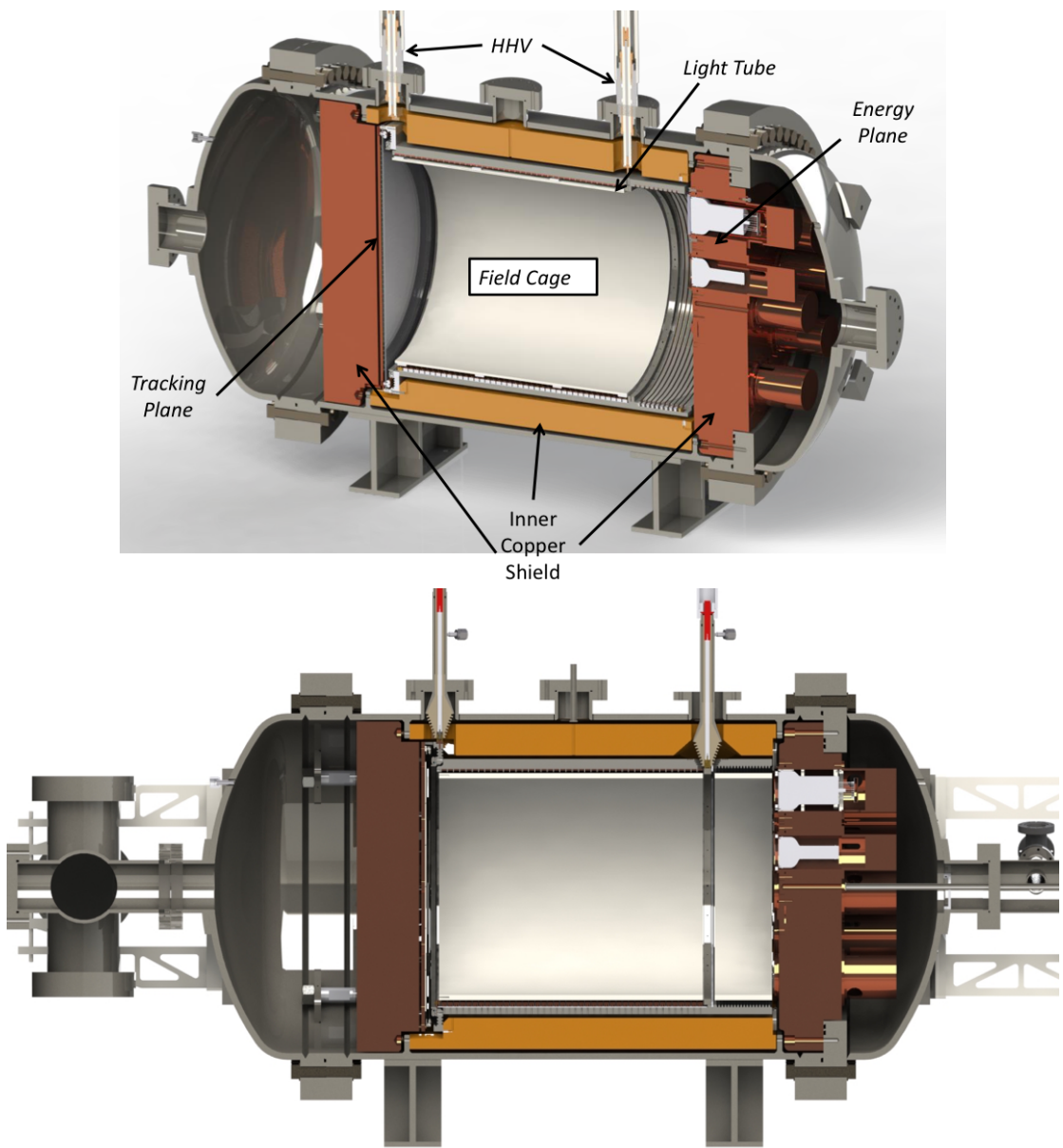


Figure 15: Top: a 3D drawing of the NEW detector. Bottom: a lateral view

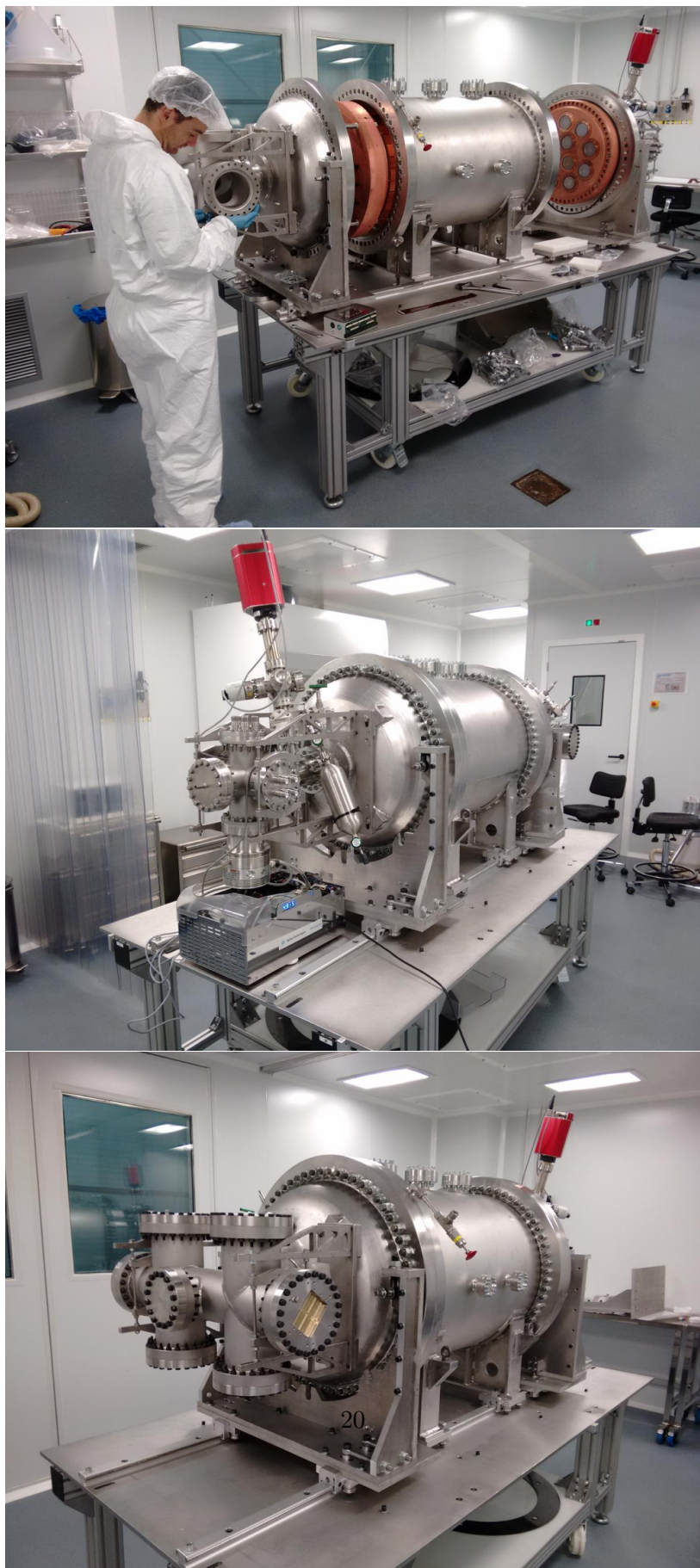


Figure 16: The NEW detector being assembled in the LSC clean room in 2015. Top: A picture from the side, showing the two end-caps open. Middle: the detector seen from the Energy Plane side. Bottom: The detector seen from the tracking plane side

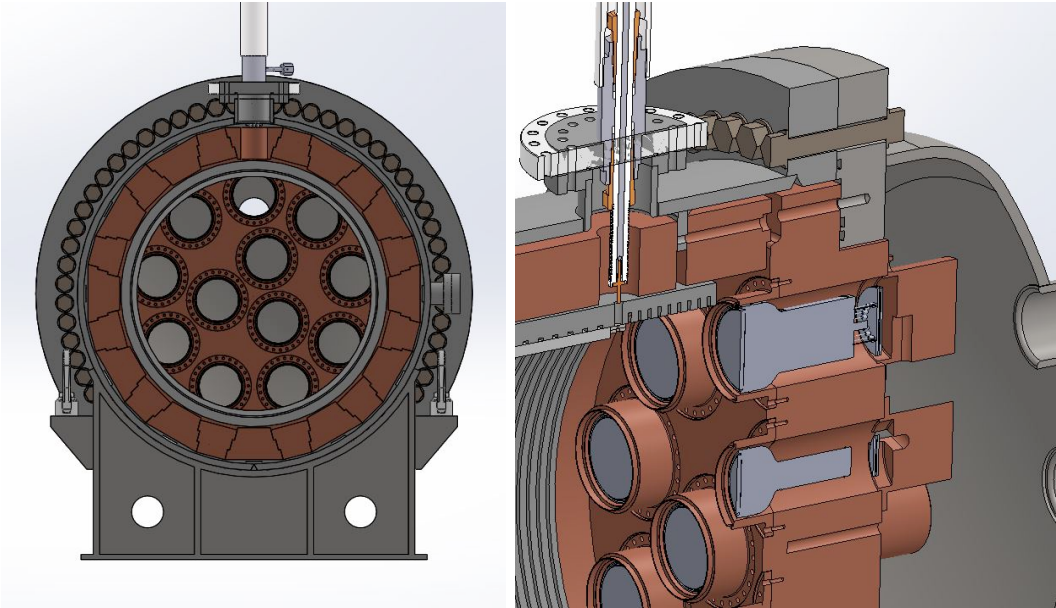


Figure 17: The NEW energy plane (EP) deploying 12 PMTs operating in vacuum and viewed by sapphire windows coated with TPB. Top: front view. Bottom: Detail showing the sapphire windows and the PMT enclosures (aka cans) terminated in thick copper caps for radiation shielding.

of a matrix of silicon photomultipliers (SiPMs) which operate as light pixels, providing a 2D picture of the event (the third coordinate is given by the drift time). The SiPMs are radiopure 1-mm sensors, manufactured by SENSL. The TP is made of 28 radiopure circuits called Kapton DICE-Boards (KDB). Each KDB has an 8×8 SiPM array, where each SiPM is placed at a 1-cm pitch. Each KDB also includes a NTC temperature sensor and one LED for calibration. The KDBs over-cover the fiducial region with ~ 1800 SiPMs, ensuring that there are no dead regions. The connector is located at the end of a long tail, and is screened from the gas, in the fiducial volume, by a 120 mm thick copper shield.

Silicon photomultipliers

A Silicon PhotoMultiplier (SiPM) consists of a matrix of photodiodes (diode which converts light into current), operating in Geiger mode. These photodiodes are connected in parallel becoming each one a pixel of the SiPM. A detailed picture of this structure is shown in figure 20. The pixels are connected by aluminum stripes to read out the combined signals, which is the sum of all pixels. The pixels are electrically decoupled by polysilicon resistive stripes between the pixels.

The SiPM used in the NEW detector are the SensL MicroFC-10035-SMT-GP model. This model has demonstrated to be sufficiently radiopure to operate in a low background experiment and also its dark current ($\sim 100\text{kHz/mm}^2$) is much lower than in the previous

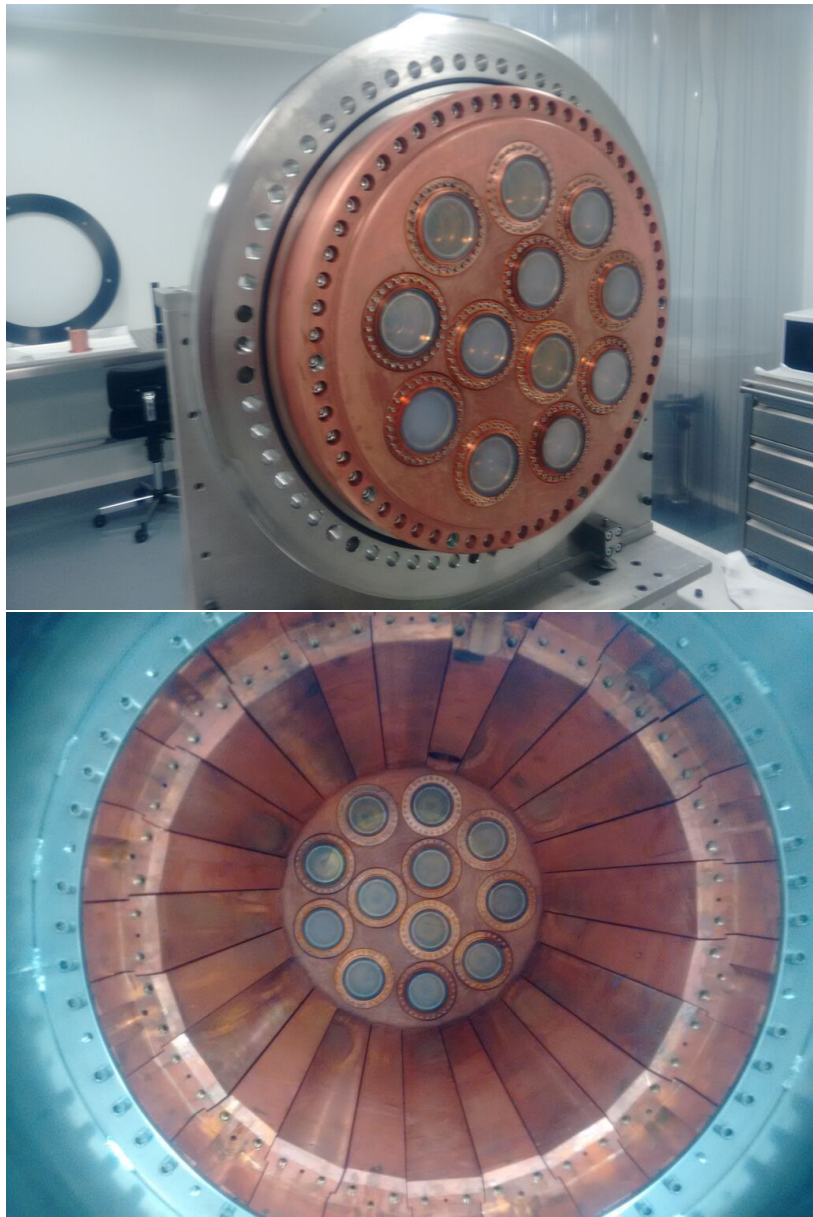


Figure 18: Assembly of the EP in 2015. Top: The end-cup plate (mother-can) with the sapphire windows already installed. Bottom: the energy plane seen from the tracking plane side. The cooper bars from the inner copper shielding, intended to attenuate the external radiation.

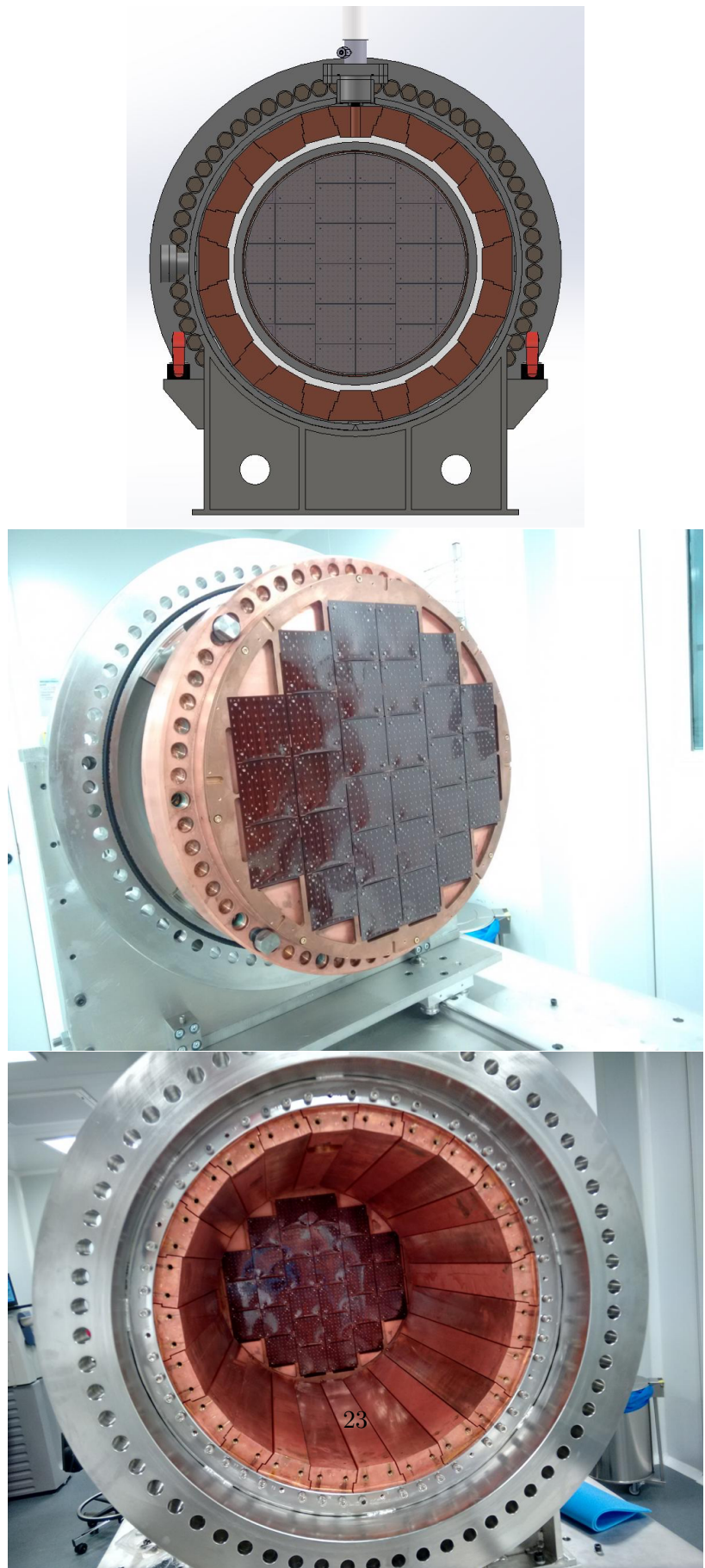


Figure 19: The NEW tracking plane. Top: A drawing, showing the KDBs over-covering the fiducial area;. Middle: The KDBs installed in the TP support plate. Bottom: The TP seen from the EP side.

models, allowing for easier calibration and an improved threshold for low energy events.



Figure 20: *Silicon photomultipliers*

KDB arrangement and cabling

A scheme of the TP cabling is shown in figure 21). The engineering problems that had to be solved were: a) to place connectors behind the copper shielding; b) to pass the KDB analog signals through custom feedthroughs; c) to transport the signals to the front-end electronics, via long-cables.

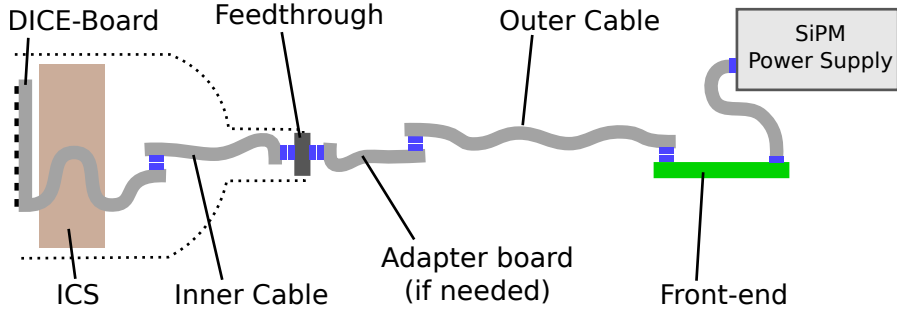


Figure 21: *Tracking plane cabling scheme.*

The KDBs where mounted on top of a thin plate of copper held by springs to the main copper plate that acts as a shielding. The reason of those springs is that they will allow for a small movement of the plate during the assembly and when closing the detector allowing for a perfect match of the tracking plane with the EL region. Fig. 22 shows the detail of one of those springs.

Once the KDBs are mounted the tail has to be passed through the holes in the shielding plate (Fig. 23). At the end of the tail a connector is soldered to plug a cable extension made of the same materials than the DICE-Boards. Those cables have to be organised to reach 5 different feed-throughs. The distribution of the cables is done using 3D printed structures placed inside a steel structure that will allow to extract the SiPMs

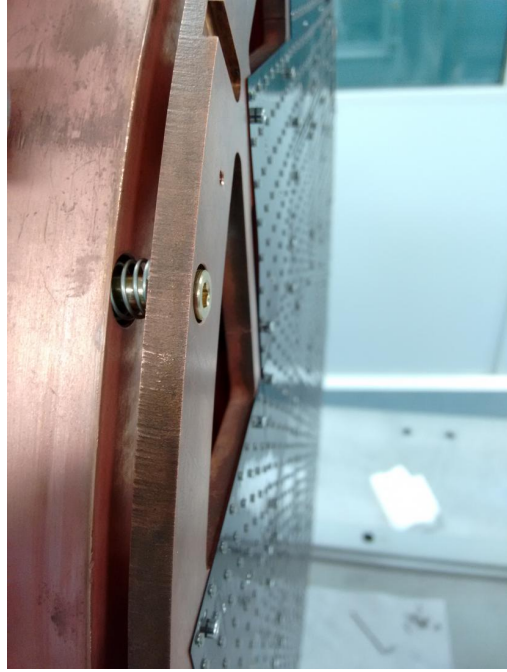


Figure 22: Detail of one of the springs in the tracking plane thin plate that will allow to accommodate the tracking plane perfectly parallel to the electroluminescence region.

cables and also is the point where the piping for vacuum and evacuation connects (Fig. 24).

The final step in the connection of inner cables of the tacking plane is the connexion to the tracking-plane feedthroughs (TPFT). Each one of these custom-made FT allows up to 6 KDB connexions. Extracting the signals of the 29 KDBs require then 5 TPFT. Figure 25 shows the front and the back side of theTPFT as well as the cable connexion.

External cabling

In order to keep background events to a minimum, front-end electronics are placed nearby the detector but beyond the lead castle that surrounds the TPC, with a total cable length of ~ 5 m from the sensor to the electronics. This poses a challenge in the design of a cabling solution that (1) is radio-clean enough to be inside the detector, (2) keeps enough signal-to-noise ratio in the relevant signal bandwidth for the gated integrator with a 5 m cable, (3) is cost-effective, (4) includes SiPM biasing voltage wires and (5) is also valid for the final NEXT phase (NEXT-100).

Differential transmission lines on fine-pitch FFC cables outside the detector were chosen as a good trade off between performance and cost. As shown in figure 26, the cables are 0.5 mm pitch with $280 \times 76\mu\text{m}$ traces embedded in a thin polyester layer. The anode and the cathode of each SiPM are connected to the *signal* and *bias* lines

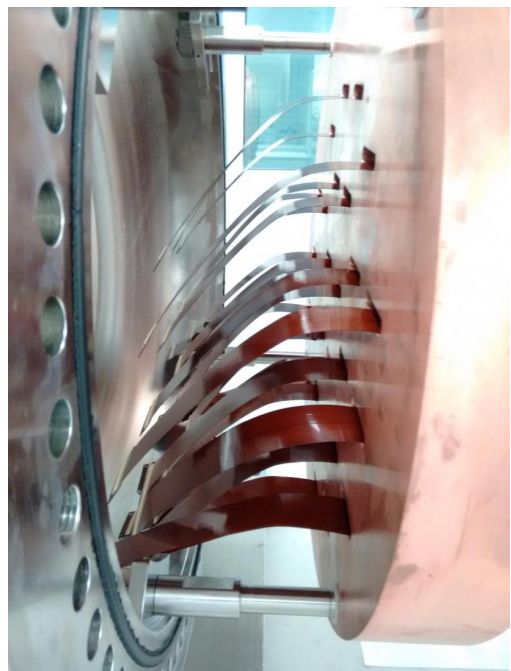


Figure 23: Dice-Boards cables passing through the holes in the shielding plate. At the end of the tail there is a connector that will allow for an extension of the cable to reach the feed-through.



Figure 24: Up left: Steel structure to support and organize the SiPM cabling. Up right: 3D printed structure to allow a better distribution of the cables. Bottom: Assembly process of the SiPM cables.

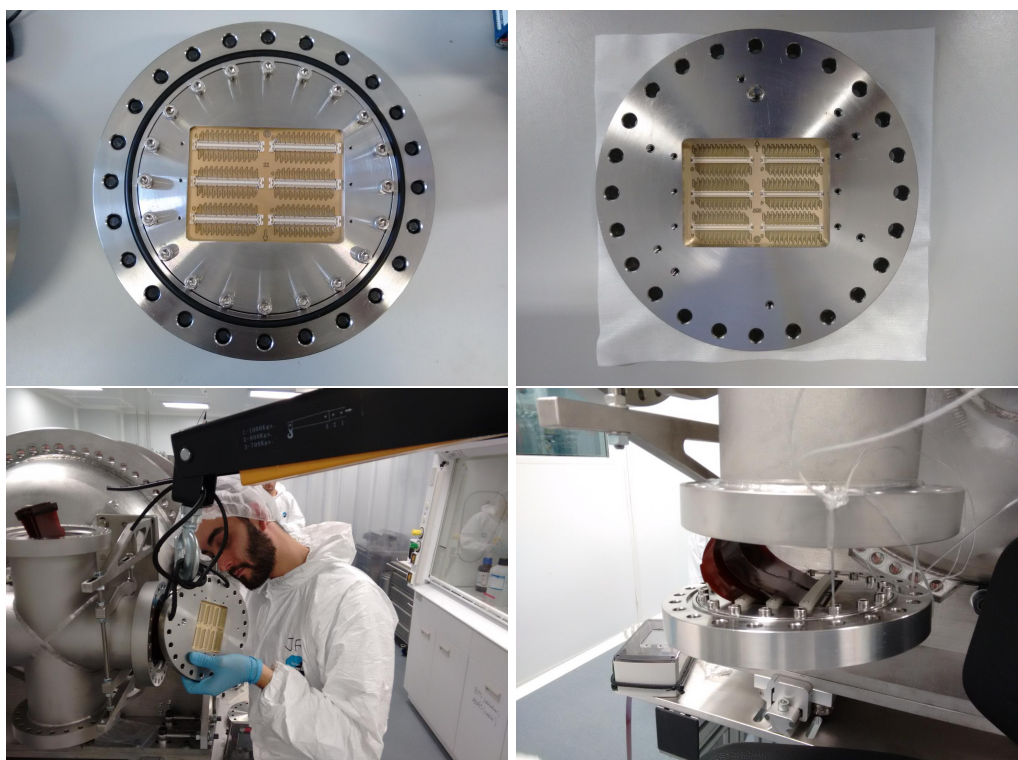


Figure 25: Up left: Inner side of the TPFT. Up right: external side of the TPFT. Bottom: Cable connexion.

respectively. Channels are separated by a guard trace connected to the analog ground in the front-end. Therefore three lines are needed for each SiPM channel. In addition, each KDB adds several more lines, for the temperature sensor and calibrating LEDs.

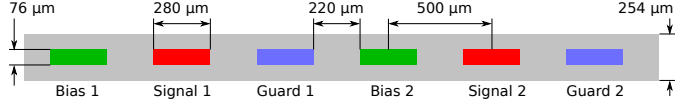


Figure 26: Cross-section of the external cable (just two channels are shown).

Since commercial cables with the required density of traces were not available, the adopted solution was to split into four FFC cables. This way, the signals of a whole DICE-Board are distributed in four cables of 51 wires each. This distribution is done just at the output of the feedthrough, using a Kapton adapter board. This board has the same stackup as the DICE-Board or the inner cable, and splits the signals in four *DF9 Hirose* connectors for the long cables.

In order to further reduce the noise coupled to the external cables, they are wrapped with a 1 mm aperture mesh, also connected to the analog ground at the front-end. This mesh is has its maximum attenuation rated at 1 MHz, which covers the range of frequencies we want to attenuate.

The external cables have been connected to the output of the TPFT and then they go below the platform until the position of the FEE boards where they are connected. (Fig. 27)

Sensor characterisation

The simplest method to calibrate the SiPMs is shown in figure 28 (top panel), and consists in finding the different peaks associated to the different photoelectron numbers in the SiPM and extract the gain according to their separation. The first results from NEW show that the gain spread among the SiPMs is very small (figure 28 bottom).

Reflectors

The material of choice for the KDBs (Kapton) as many advantages including flexibility, little degassing and radiopurity. However it is a poor reflector. In order to increase the amount of light recorded by the energy plane, a 2 mm teflon reflector is placed in front of each KDB. The reflectors (Fig. 29) have holes to accommodate the SiPMs without damaging them and also have a space for the thermal sensor and the LEDs. However no holes are neccesary for the LEDs, since teflon is sufficiently transparent to the blue light they emit.

3.3 Field Cage

The main body of the field cage (figure 30) is a high-density polyethylene (HDPE) cylindrical shell that provides electric insulation from the vessel. The shell is 2.5 cm

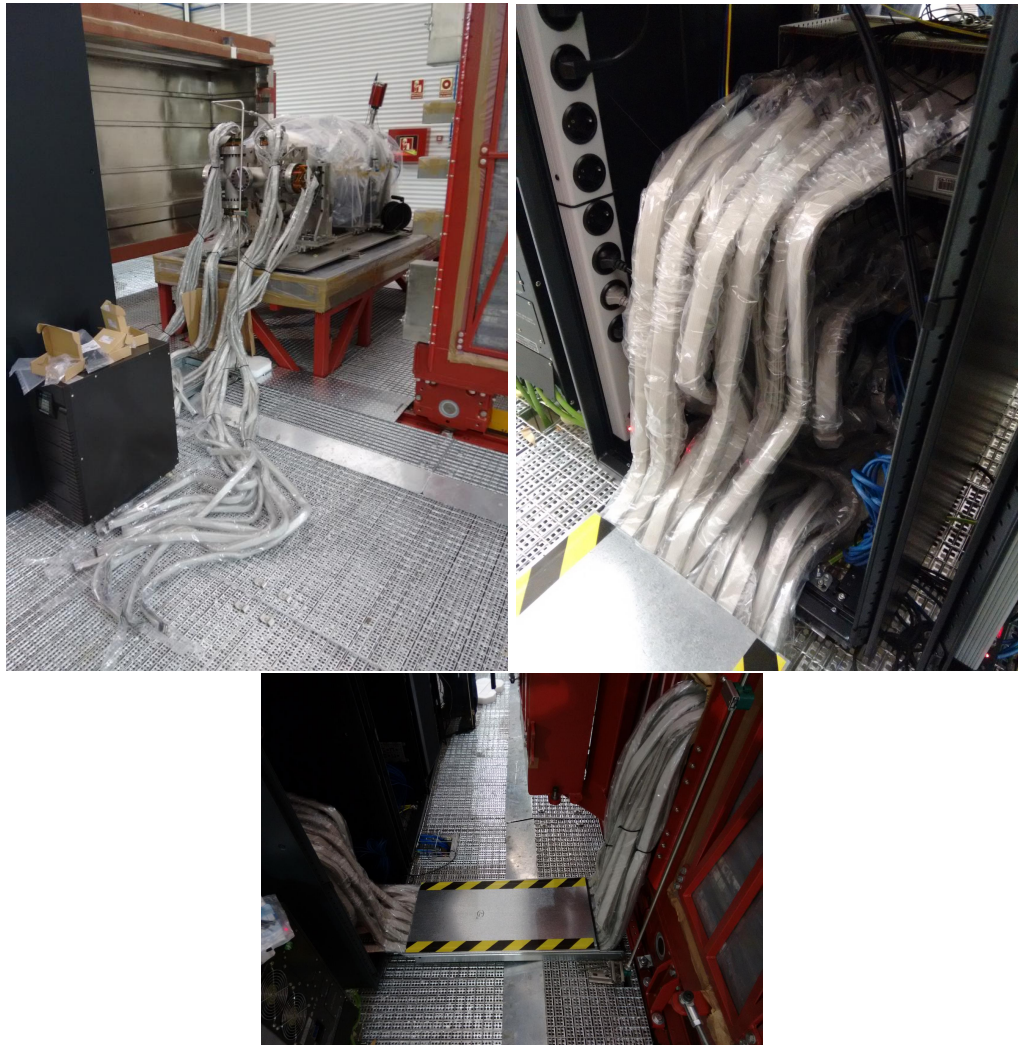


Figure 27: Different parts of the external cabling of the tracking plane. Up left shows a general view of the cabling. Up right picture is a detail of the connexion of the cables to the FEE boards. Bottom picture shows how the cables move under the platform.

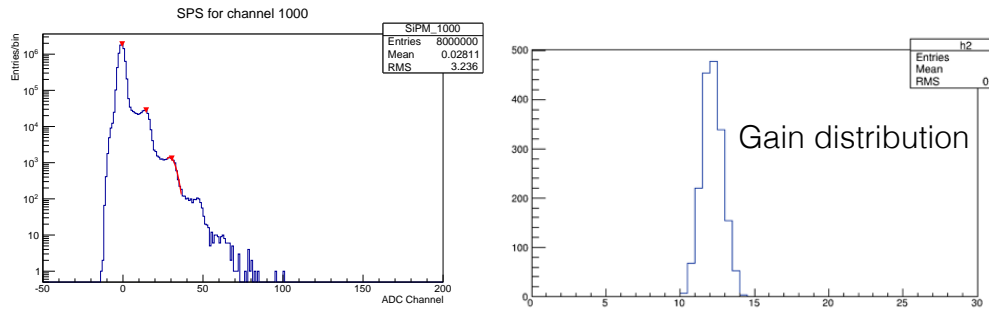


Figure 28: Top: standard method for calibration where the charge corresponding to the different number of photoelectrons in the SiPMs is estimated with a fit to the peak. The gain of the SiPM is calculated using the separation of the different peaks. Bottom: Histogram showing the gain of all the SiPMs in the plane. This histogram shows that the spread on the SiPMs gain is only of the order of a few ADC counts.

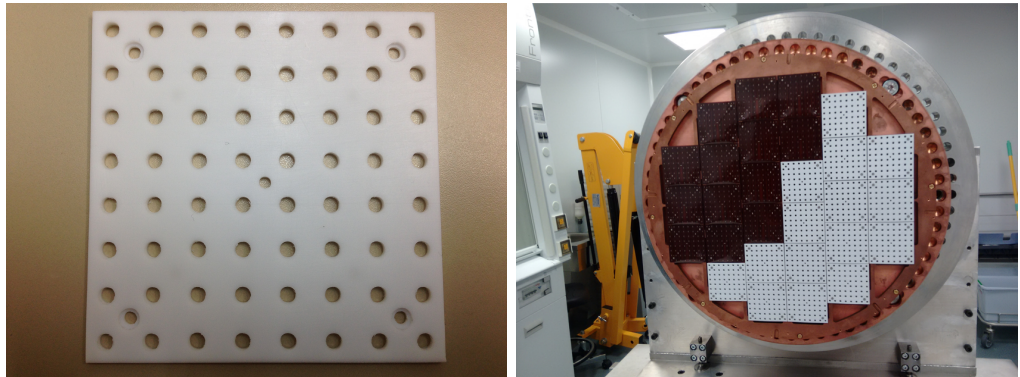


Figure 29: Top: Front side (EL) of the reflector. Bottom: The TP with half covered with the reflectors.

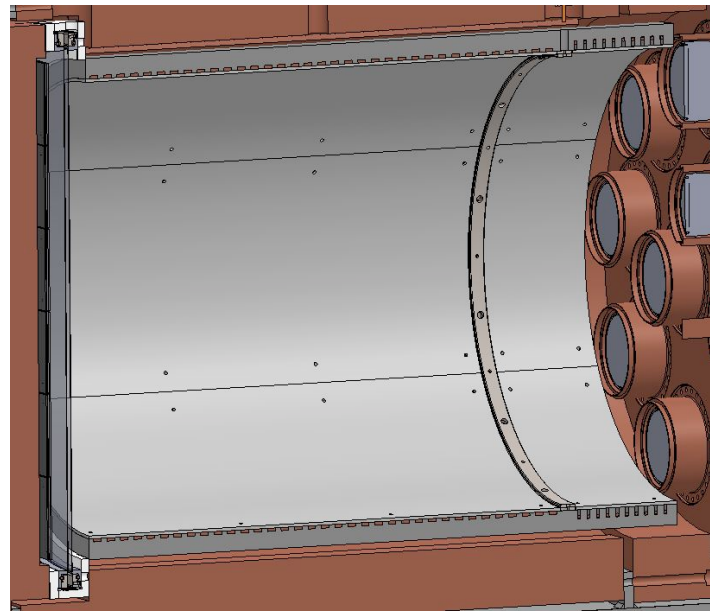


Figure 30: The NEW field cage (NFC).

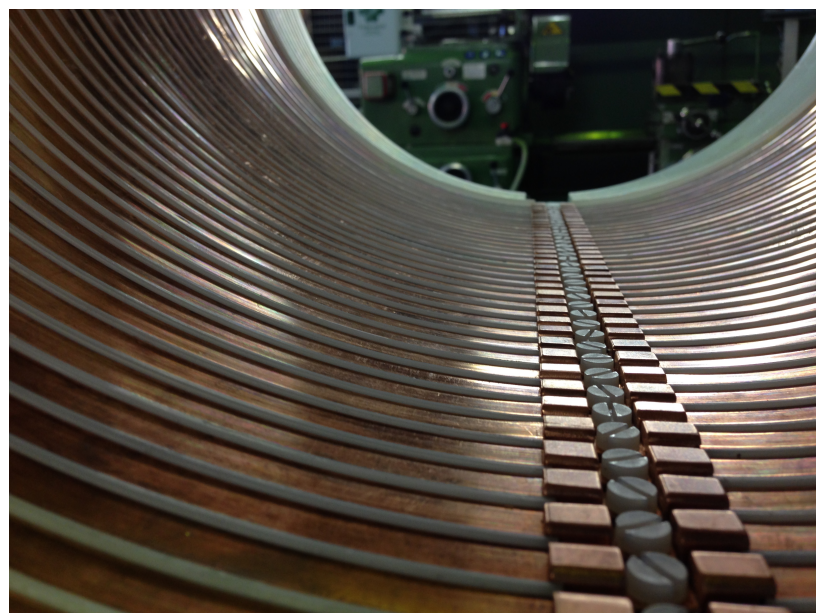


Figure 31: Detail of the copper rings in the drift region.

thick. Two wire meshes (cathode and anode) define the active volume of NEW. The electroluminescence region is defined by one of these meshes (cathode) and a fused silica plate (gate) with an ITO coating to make its surface resistive (gate). Ultra pure copper strips attached to the HDPE and connected with low background 10G? resistors (figure 31) grade the high voltage to provide a homogeneous and uniform moderate electric field (300-600 V/cm) inside the active volume of the NEW detector. The goal of the FC is to provide an homogeneous and uniform electric field inside the active volume of the NEW detector. The field cage has an outer diameter (OD) of 50 cm and a length of 50 cm. Thus, both the longitudinal and radial dimensions are roughly half of those of NEXT-100.

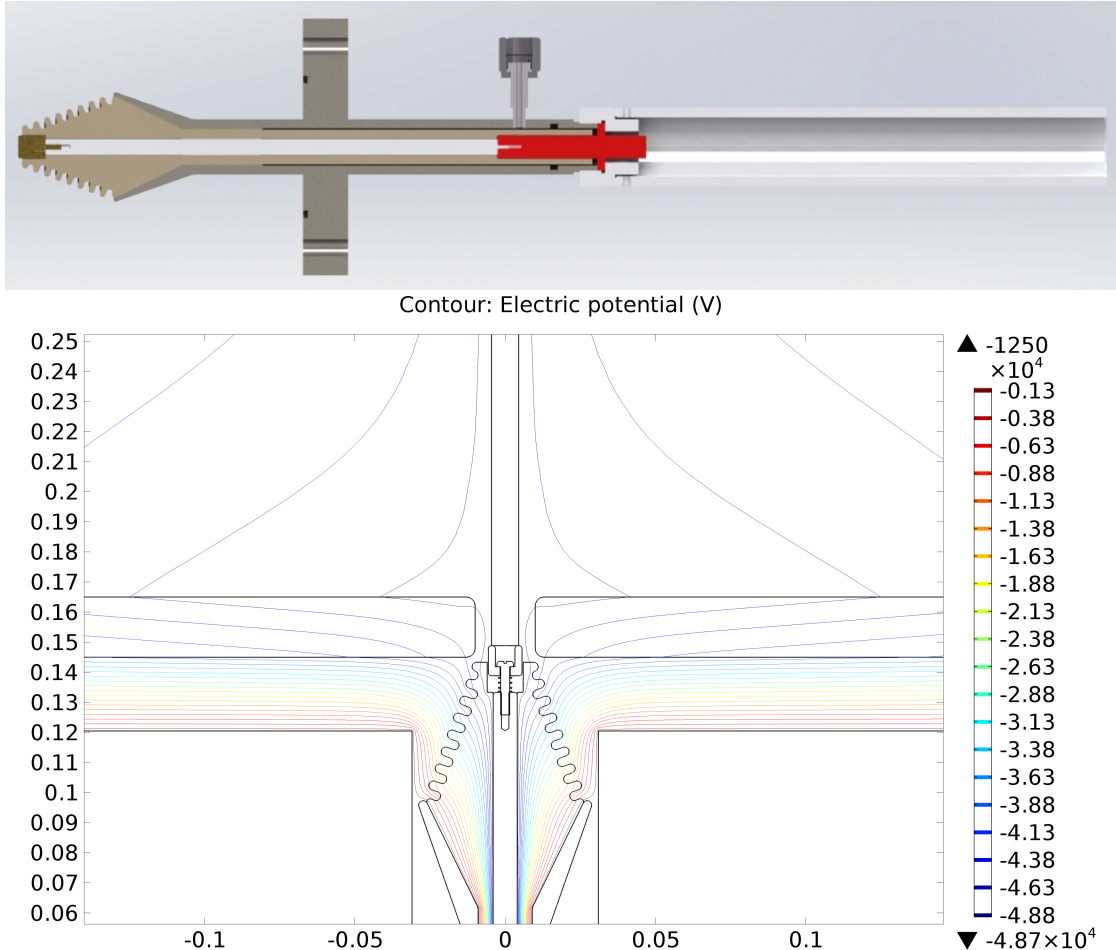


Figure 32: Design (top) and Comsol simulation (bottom) of the NEW HVFT.

The most challenging parts of the field cage are the high voltage feedthroughs. These are penetrators which must be capable of holding very high voltages (up to 50 kV for the cathode penetrator and up to 20 kV for the anode) while at the same time being radiopure and gas tight. Figure 32 shows the design of the NEW HVFT. Figure 34 shows

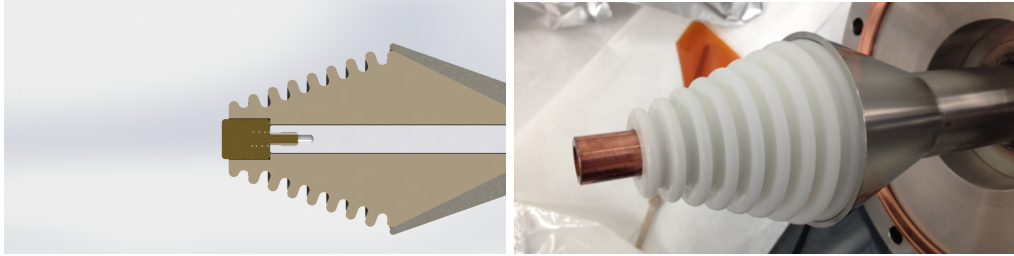


Figure 33: Detail of the HVFT tip. The copper connector has been designed to minimise the electric field in the surface of the tip. Right: picture of the HVFT.

Figure 34: Detail of the HVFT tip. The copper connector has been designed to minimise the electric field in the surface of the tip.

a detail of the tip (left) and a picture of the cathode HVFT. The initial tests show that the HVFT can hold a voltage in excess of 30 kV with only a few sparks a day. Work is in progress to reduce the number of sparks and increase the maximum voltage. However, 30 kV is sufficient for the initial period of commissioning at 10 bar with a drift field of 15 kV (300 V/cm over 50 cm) and en EL voltage of 15 kV. ($E/P \sim 3$). For NEXT-100 the HVFT needs to withstand 45-55 kV (depending on pressure and EL). Operation with NEW will be essential to improve the performance of the HVFT.

The cathode grid consist of a stainless steel frame with wires to fix the potential (figure 35). It has been built by the University of Texas A&M and is currently at the LSC, ready to be installed (first week of May, 2016)..



Figure 35: Cathode frame (left) with a detail of the groves for fixing the wires. The bronze tensioners (left) will be used to strength avery wire at the right tension.

The electroluminescent region (EL) is the amplification region of the detector (figure 36). The main parts of the EL are the mesh and the anode. The anode consists in a plate of fused silica coated with ITO in one side and TPB in the other. The fused silica with the layer ITO was produced by Texas A&M and it arrived at the end of May 2015. It was coated at the LNGS coating facilities and it is ready for installation. The gate



Figure 36: Top pictures show the different frames used for assembly and tension the gate mesh. Bottom is a picture of the fused silica plate before coating with ITO

mesh is also ready for installation.

4 Conclusions

A progress report of the NEXT project, has been presented. The report describes the progress in the construction and commissioning of the experiment infrastructures and the NEW detector during 2015 and the first quarter of 2016. In summary:

- The working platform, seismic pedestal and lead castle are completed and operational.
- The full NEXT gas system, including recirculation, purification, emergency storage and cryo-recovery is ready to be certified for operation (scheduled for May, 2016).
- The NEW detector is being assembled at the LSC. The energy plane and tracking plane are already installed and the field cage is scheduled for installation in May, 2016.
- The collaboration is completing the risk assessment needed for regular operation at the LSC.
- The Slow Controls are ready to operate.
- The plan for the second semester of 2016 is to commission the detector, identifying technical issues and ensuring the stability and reliability of the apparatus and gas system.
- The set of measurements foreseen for the initial operation period include the measurement of the electron lifetime, and calibrations with LEDs and radioactive sources.
- The calibration aims at producing a first measurement of the NEW energy resolution by the November, 2016, LSCSC meeting.

References

- [1] **NEXT** Collaboration, V. Alvarez et al., *NEXT-100 Technical Design Report (TDR): Executive Summary*, *JINST* **7** (2012) T06001, [[arXiv:1202.0721](https://arxiv.org/abs/1202.0721)].
- [2] **NEXT** Collaboration, E. D. C. Freitas et al., *PMT calibration of a scintillation detector using primary scintillation*, *JINST* **10** (2015), no. 02 C02039.
- [3] **NEXT** Collaboration, V. Alvarez et al., *Radiopurity control in the NEXT-100 double beta decay experiment: procedures and initial measurements*, *JINST* **8** (2012) T01002, [[arXiv:1211.3961](https://arxiv.org/abs/1211.3961)].

- [4] **NEXT** Collaboration, S. Cebrian et al., *Radiopurity assessment of the tracking readout for the NEXT double beta decay experiment*, *JINST* **10** (2015), no. 05 P05006, [[arXiv:1411.1433](#)].
- [5] S. Cebrian et al., *Radon and material radiopurity assessment for the NEXT double beta decay experiment*, *AIP Conf. Proc.* **1672** (2015) 060002, [[arXiv:1505.0705](#)].
- [6] R. Esteve, J. Toledo, F. Monrabal, D. Lorca, L. Serra, et al., *The trigger system in the NEXT-DEMO detector*, *JINST* **7** (2012) C12001.
- [7] A. Gil, J. Diaz, J. Gómez-Cadenas, V. Herrero, J. Rodriguez, et al., *Front-end electronics for accurate energy measurement of double beta decays*, *Nucl. Instrum. Meth. A* **695** (2012) 407–409.
- [8] **NEXT** Collaboration, V. Alvarez et al., *Near-Intrinsic Energy Resolution for 30 to 662 keV Gamma Rays in a High Pressure Xenon Electroluminescent TPC*, *Nucl. Instrum. Meth. A* **708** (2012) 101–114, [[arXiv:1211.4474](#)].
- [9] **The NEXT Collaboration** Collaboration, V. lvarez et al., *Operation and first results of the NEXT-DEMO prototype using a silicon photomultiplier tracking array*, [arXiv:1306.0471](#).
- [10] **NEXT** Collaboration, V. Álvarez et al., *Ionization and scintillation response of high-pressure xenon gas to alpha particles*, *JINST* **1305** (2013) P05025, [[arXiv:1211.4508](#)].
- [11] **NEXT** Collaboration, D. Lorca et al., *Characterisation of NEXT-DEMO using xenon K_α X-rays*, *JINST* **9** (2014), no. 10 P10007, [[arXiv:1407.3966](#)].
- [12] **The NEXT collaboration** Collaboration, V. Alvarez et al., *Characterization of a medium size Xe/TMA TPC instrumented with microbulk Micromegas, using low-energy γ-rays*, [arXiv:1311.3535](#).
- [13] **NEXT Collaboration** Collaboration, V. lvarez et al., *Description and commissioning of NEXT-MM prototype: first results from operation in a Xenon-Triethylamine gas mixture*, [arXiv:1311.3242](#).
- [14] **NEXT** Collaboration, J. Renner et al., *Ionization and scintillation of nuclear recoils in gaseous xenon*, *Nucl. Instrum. Meth. A* **793** (2015) 62–74, [[arXiv:1409.2853](#)].
- [15] **NEXT** Collaboration, L. Serra et al., *An improved measurement of electron-ion recombination in high-pressure xenon gas*, *JINST* **10** (2015), no. 03 P03025, [[arXiv:1412.3573](#)].
- [16] **NEXT** Collaboration, P. Ferrario et al., *First proof of topological signature in the high pressure xenon gas TPC with electroluminescence amplification for the NEXT experiment*, *JHEP* **01** (2016) 104, [[arXiv:1507.0590](#)].

- [17] J. Gómez-Cadenas, J. Martín-Albo, and F. Monrabal, *NEXT, high-pressure xenon gas experiments for ultimate sensitivity to Majorana neutrinos*, *JINST* **7** (2012) C11007, [[arXiv:1210.0341](https://arxiv.org/abs/1210.0341)].
- [18] **NEXT** Collaboration, J. Martín-Albo and J. J. Gómez-Cadenas, *Status and physics potential of NEXT-100*, [arXiv:1301.2966](https://arxiv.org/abs/1301.2966).
- [19] **NEXT Collaboration** Collaboration, J. Gomez-Cadenas et al., *Present status and future perspectives of the NEXT experiment*, [arXiv:1307.3914](https://arxiv.org/abs/1307.3914).
- [20] **NEXT** Collaboration, J. Martin-Albo et al., *Sensitivity of NEXT-100 to neutrinoless double beta decay*, [arXiv:1511.0924](https://arxiv.org/abs/1511.0924).